
A LOWER BOUND FOR THE ELBO OF THE BERNOULLI VARIATIONAL AUTOENCODER

TECHNICAL REPORT

Robert Sicks*¹ Ralf Korn² Stefanie Schwaar¹

¹Department of Financial Mathematics, Fraunhofer ITWM, Kaiserslautern, Germany

²Department of Financial Mathematics, Technical University of Kaiserslautern, Kaiserslautern, Germany

March 27, 2020

ABSTRACT

We consider a variational autoencoder (VAE) for binary data. Our main innovations are an interpretable lower bound for its training objective, a modified initialization and architecture of such a VAE that leads to faster training, and a decision support for finding the appropriate dimension of the latent space via using a PCA. Numerical examples illustrate our theoretical result and the performance of the new architecture.

Keywords Logistic PCA, Bernoulli distribution, Initialization, Variational Autoencoder

1 Introduction

With the Variational Autoencoder (VAE), [Kingma and Welling, 2014] present a special form of autoencoder that incorporates randomness to the architecture. This form of autoencoder yields an interpretable latent space when it comes to images as input. [Goodfellow et al., 2016] describe VAE as an “excellent manifold learning algorithm” due to the fact that the model is forced “to learn a predictable coordinate system that the encoder can capture”. Furthermore, VAE are suitable for generating new unobserved data by interpolating within the latent space (see the appendix A in [Kingma and Welling, 2014] for vivid examples of moving through the latent space).

In this paper we analyse VAE for the case of binary data. Let $x^{(1)}, \dots, x^{(N)} \in \{0, 1\}^d$ be such observations. A VAE consists of an encoder and a decoder. The encoder maps these multivariate binary observations to a low-dimensional numeric space of dimension $\kappa \ll d$. The decoder applies the inverse operation. [Kingma and Welling, 2014] introduce the “Bernoulli MLP decoder” for the binary setting used here. We call a VAE with this type of decoder “Bernoulli VAE”.

This work contributes to the understanding of VAE in three areas:

1. We derive an interpretable lower bound for the training objective of a Bernoulli VAE (the ELBO).
2. We propose an initialization scheme with an architecture change for Bernoulli VAE that results in faster convergence.
3. We derive a decision support for finding the parameter of the latent space dimension κ with a principal component analysis (PCA).

Probably the most comparable work in this research field is [Lee et al., 2010]. They present a sparse logistic PCA, which has a target objective similar to the Bernoulli VAE: A balance between the reconstruction of the binary inputs and a regularization term. [Kunin et al., 2019] show that regularization helps the linear autoencoder to learn principal directions. Without regularization the linear autoencoder learns the subspace spanned by the top principal

*Corresponding author

direction but not the directions themselves. [Dai et al., 2018] provide an interpretable term for the ELBO of a VAE with a ‘‘Gaussian MLP decoder’’ (as denoted in [Kingma and Welling, 2014]). This term is similar to our bound. [Tipping and Bishop, 1999] derive an equivalent term, again under Gaussian assumptions but from the perspective of a PCA instead of a VAE.

For this paper, we assume X_1, \dots, X_d given Z to be mutually independent and Bernoulli distributed. This assumption yields what is known as the ‘‘Cross Entropy Loss’’. This loss finds application in different fields: [Blaschke et al., 2018] apply VAE on molecules represented in a so-called ‘‘SMILE’’-format. [Germain et al., 2015] develop a modification for autoencoders to consider autoregressive constraints and focus on binary inputs. [Duan et al., 2019] apply the Bernoulli VAE to images.[†]

This article is structured as follows: In section 2, we present related work and compare our mathematical problem in detail to the existing literature. Theoretical findings and discussion can be found in section 3. In section 4, we look at our simulation setup and present our results. Finally, we summarize in section 5 our contribution to the research of VAE and highlight further research topics.

2 Background and related work

The Bernoulli VAE yields a continuous representation of binary data, which can be viewed as a kind of logistic PCA. In this chapter, we have a look at related work and compare the mathematical formulations of sparse logistic PCA and Bernoulli VAE.

2.1 Related work: Logistic PCA

[Tipping and Bishop, 1999] view PCA as a maximum likelihood procedure and introduce it as a probabilistic PCA (pPCA). We show connections of the Bernoulli VAE to pPCA based on our bound. [Collins et al., 2002] generalize pPCA and derive an optimization for the exponential family. They provide a generic algorithm for minimizing the loss. [de Leeuw, 2006] presents logistic (and probit) forms of PCA and a majorization algorithm to fit the parameters. [Lee et al., 2010] propose a sparse logistic PCA by introducing L_1 regularization. This can be seen as the deterministic version of our proposed method here as we will see in section 2.3. [Landgraf and Lee, 2015] formulate the logistic PCA differently: For binary data their model is not based on matrix-factorization but on projection of the data.

2.2 Related work: Autoencoder

[Bourlard and Kamp, 1988] show for autoencoders with linearizable activations that the optimal solution is given by the solution of a Singular Value Decomposition. [Baldi and Hornik, 1989] extend these results and analyse the squared error loss of autoencoders for all critical points. [Saxe et al., 2014] provide theory for learning deep linear neural networks for different non-linear dynamics. [Josse and Wager, 2016] present an autoencoder that provides a stable encoding when perturbed with bootstrap noise. Therefore, it can adapt to non-isotropic noise structures. [Pretorius et al., 2018] analyse the learning dynamics of linear denoising autoencoders. [Dai et al., 2018] analyse the loss of the Gaussian VAE. They show connections to pPCA and robust PCA. The bound of the ELBO from this paper has an equivalent form to one of their results. [Kunin et al., 2019] consider regularizations in linear autoencoders and analyse the critical points for three targets.

VAE experience regularization over the Kullback-Leibler-Divergence (KL-Divergence) term (see below). Variations of autoencoders exists, which regularize the closeness of distributions in a different way. Adversarial Autoencoders (AAE) (see [Makhzani et al., 2015]) try to approximate the Jensen-Shannon-Divergence instead of using the KL-Divergence. [Zhao et al., 2019] motivate a unifying model for VAE and AAE.

2.3 Comparison of sparse logistic PCA and Bernoulli VAE

We are interested in a sparse low-rank representation of binary data. One possible approach is the logistic PCA introduced by [Lee et al., 2010]. Let $x^{(1)}, \dots, x^{(N)} \in \{0, 1\}^d$ be the observations of X , a multivariate Bernoulli distributed random variable, having a low-rank representation. Let $(a^{(1)}, \dots, a^{(N)})^T = A \in \mathbb{R}^{N \times \kappa}$ denote these representations with $\kappa \ll d$, i.e. there exists $(b_1 | \dots | b_\kappa) = B \in \mathbb{R}^{d \times \kappa}$ and a location vector $\vec{b}_0 \in \mathbb{R}^d$ such that

$$P(X = x^{(i)}) \sim \text{Bern} \left(p(\vec{b}_0, a^{(i)}, B) \right),$$

[†]Even though images are usually not represented in binary fashion, the pixel range can be transformed to be within zero and one. E.g. if the values originally range from 0 to 255 we divide them by 255.

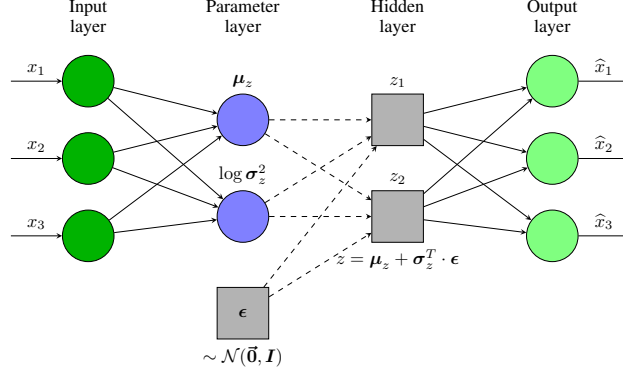


Figure 1: The implementation of a VAE as a neural net. The outputs on the right side should resemble the inputs on the left as good as possible. The solid arrows in the picture stand for the biases and weights. The dashed arrows correspond to the calculation procedure $z = \mu_z + \sigma_z^T \cdot \epsilon$. The most important feature of a VAE compared to a normal autoencoder is the stochastic source, from which we sample to get an output. Note that “ μ_z ” and “ $\log \sigma_z^2$ ” are κ -dimensional and (for this picture) we assume an independent Gaussian distribution of Z .

where $p(\vec{b}_0, a^{(i)}, B) \in [0, 1]^d$ denotes the probability vector. Finding the sparse low-rank representation (in the spirit of [Lee et al., 2010]) leads to maximizing the log-likelihood and a penalization term, given by

$$\ell(\vec{b}_0, A, B) - N \cdot P_\lambda(B). \quad (1)$$

[Lee et al., 2010] introduced a L_1 penalty term to get sparse loading vectors b_1, \dots, b_κ , similar to the LASSO regression from [Tibshirani, 1996].

We are going to analyse an alternative to logistic PCA using the VAE introduced by [Kingma and Welling, 2014]. For the VAE setup, we add a latent variable Z with density $q_\phi(z|X)$ to this model. We change our perspective from

$$P(X = x^{(i)}) \sim \text{Bern} \left(p(\vec{b}_0, a^{(i)}, B) \right),$$

to

$$P_\theta(X|Z) \sim \text{Bern} (p_\theta(Z)),$$

where the probability vector $p_\theta(Z) \in [0, 1]^d$ is a function of Z and the model parameters θ . We interpret this as replacing the deterministic low-rank representation $a^{(i)}$ by a stochastic $z^{(i)}$.

Using the Bayes theorem, we get

$$\ln P_\theta(x^{(i)}) \geq \mathbb{E}_{q_\phi(\cdot|x^{(i)})} \left[\log P_\theta(x^{(i)}|Z) \right] - D_{KL} \left(q_\phi(Z|x^{(i)}) || p(Z) \right),$$

which gives a lower bound for the log-likelihood function: The “Evidence Lower Bound” (ELBO). Since in our current model formulation the log-likelihood is intractable, we maximize the ELBO instead and assume the corresponding log-likelihood to increase as well.

The first part $\mathbb{E}_{q_\phi(\cdot|x)} [\log P_\theta(x|Z)]$ resembles the reconstruction error of an autoencoder: Given a sample $z \sim q_\phi(\cdot|x)$, we integrate over the probabilities that an observation x was generated from that sample. The expression $q_\phi(\cdot|x)$ is the generating function that resembles the encoder in the autoencoder. $P_\theta(x|Z)$ can be identified with the decoder of an autoencoder. Both, encoder and decoder are usually implemented as a multi layer perceptron (MLP). The second term is the Kullback-Leibler-Divergence that indicates how close the two inputs are. The further these two expressions are apart, the higher the penalization. Figure 1 shows the implementation of a VAE as a neural net.

There are several similarities to the work of [Lee et al., 2010]:

- The ELBO and the loss in (1) consist of two parts: The first part provides information on the goodness of fit, while the second part is a penalty term.
- To minimize the loss in (1) [Lee et al., 2010] use a “Majorization-Minimization”, algorithm based on a second order Taylor series expansion. For the proof of proposition 1, we also use a second order Taylor series expansion.
- The probability vector of [Lee et al., 2010] $p(\vec{b}_0, a^{(i)}, B)$ and our assumed probability vector $p_\theta(Z)$ use sigmoid activation.

3 Theoretical results

In this section, we present our theoretical findings. Recall that

$$\ln P_{\theta}(x^{(i)}) \geq ELBO.$$

Our central result is the lower bound for the ELBO in proposition 1. So instead of the ELBO, we maximize the lower bound and assume that the corresponding log-likelihood increases.

We first state our setting and assumptions. Then we formulate proposition 1 and interpret the resulting lower bound of the ELBO. Based on these findings, we introduce an initialization and a change of architecture for Bernoulli VAE. Finally, we propose a way to determine the latent space dimension κ given the training data.

3.1 Assumptions and lower bound

Let $x^{(1)}, \dots, x^{(N)} \in \{0, 1\}^d$ denote the observations, where $d \in \mathbb{N}$ denotes the dimension. We assume a latent variable model: The values $x^{(1)}, \dots, x^{(N)}$ were generated given a latent (not observable) sample z of a κ -dimensional variable Z . Furthermore, we assume $d \gg \kappa$ and X_1, \dots, X_d given Z are mutually independent. The distribution of X given Z is

$$P_{\theta}(X|Z) \sim \text{Bern}(p_{\theta}(Z)), \quad (2)$$

where the probability vector $p_{\theta}(Z) \in [0, 1]^d$ is a function of Z and the model parameters θ . We fix the probability vector $p_{\theta}(Z)$ the following way: For each entry of $p_{\theta}(z) \in [0, 1]^d$, we have

$$p_{\theta,j}(Z) := \sigma([WZ + b]_j) = \frac{1}{1 + e^{-[WZ + b]_j}}$$

with $W \in \mathbb{R}^{d \times \kappa}$, $b \in \mathbb{R}^d$ and $[\cdot]_j$ the j -th entry. $\sigma(\cdot)$ is the sigmoid function. Hence $\theta := \{W, b\}$ in our case. W and b can be identified with the weights and biases of the decoder of the VAE. In figure 1, these are the arrows between ‘‘Hidden Layer’’ and ‘‘Output Layer’’.

We further expect the distribution of the variables Z to be given by the standard recognition model (see [Kingma and Welling, 2014]):

$$q_{\phi}(z|X) \sim \mathcal{N}(\mu_z, \Sigma_z),$$

where we define μ_z and Σ_z as functions of X and ϕ . Furthermore, we define $p(z)$ as the density of a standard normal distribution $\mathcal{N}(\mathbf{0}, \mathbf{I})$.

The target of a VAE is the average ELBO, given by

$$\mathcal{L}(\phi, \theta) := \frac{1}{N} \sum_{i=1}^N \left(\mathbb{E}_{Z \sim q_{\phi}(\cdot|x^{(i)})} \left[\log P_{\theta}(x^{(i)}|Z) \right] - D_{KL} \left(q_{\phi}(Z|x^{(i)}) || P(Z) \right) \right), \quad (3)$$

for which we state the following lower bound:

Proposition 1. *Given the assumptions stated above, we further assume that for the encoder we have*

- $\mu_z^{(i)} := f_1(x^{(i)}, \phi)$ and
- $0 \prec \Sigma_z^{(i)} := S_z^{(i)} S_z^{(i)T}$, with $S_z^{(i)} := f_2(x^{(i)}, \phi)$,

where f_1 and f_2 are arbitrary functions that include affine transformations. Then, there exists a lower bound for the average ELBO in (3) that admits an optimal solution for $\mu_z^{(i)}$ and $\Sigma_z^{(i)}$ such that it can be written as

$$\widehat{\mathcal{L}}(W, b) = \frac{1}{N} \sum_{i=1}^N \left[-\frac{1}{2} \left(4y^{(i)} - b \right)^T C^{-1} \left(4y^{(i)} - b \right) \right] - \frac{1}{2} \log |C| + \frac{d}{2}, \quad (4)$$

where $y^{(i)} := x^{(i)} - \frac{1}{2} \mathbf{1} \in \left\{ -\frac{1}{2}, \frac{1}{2} \right\}^d$ with $\mathbf{1} := (1, \dots, 1)^T \in \mathbb{R}^d$ and $C := (4I_d + WW^T)$.

The proof of this result can be found in the supplementary material. The advantage of this lower bound is the gain in interpretability as we will see. The assumptions of proposition 1 for $\mu_z^{(i)}$ and $\Sigma_z^{(i)}$ can be interpreted as ‘‘the encoder is always doing its job’’. These are the same as in lemma 1 of [Dai et al., 2018].

The resulting objective is equivalent to the result of lemma 1 in [Dai et al., 2018] and the log-likelihood objective in [Tipping and Bishop, 1999]. Contrary to our Bernoulli distribution assumption here, their objective originated from a Gaussian distribution. Nonetheless both assume a latent variable model, as we do here. The properties derived by [Dai et al., 2018] and [Tipping and Bishop, 1999] apply to our target (4). Therefore, if we assume Σ_z to be diagonal (which is a standard assumption for VAE) we get an upper bound for (4) (see [Dai et al., 2018]).

In the following we look at the optimal values of W and b for (4) and highlight important properties. To do so, we rewrite (4) in the form of the objective in [Tipping and Bishop, 1999]:

$$\widehat{\mathcal{L}}(W, b) = \frac{1}{2} (d - \ln |C| - \text{tr}(C^{-1}S)),$$

with

$$S := \frac{1}{N} \sum_{i=1}^N (4y^{(i)} - b) (4y^{(i)} - b)^T \quad (5)$$

the sample covariance matrix (of $4y^{(i)}$), since according to [Tipping and Bishop, 1999] the maximum point for b is given by the sample mean (of $4y^{(i)}$), as follows:

$$\hat{b} = 4\bar{y} := \frac{4}{N} \sum_{i=1}^N y^{(i)}. \quad (6)$$

The maximum point for $\widehat{\mathcal{L}}$ w.r.t. W is given by

$$\widehat{W} = U_\kappa (K_\kappa - 4I_\kappa)^{1/2} R, \quad (7)$$

where $U_\kappa \in \mathbb{R}^{d \times \kappa}$ is composed of κ eigenvectors of the matrix S . These eigenvectors are associated with the κ biggest eigenvalues $\lambda_1, \dots, \lambda_\kappa$. $K_\kappa \in \mathbb{R}^{\kappa \times \kappa}$ is a diagonal matrix with entries

$$k_j = \begin{cases} \lambda_j, & \lambda_j \geq 4 \\ 4, & \text{else} \end{cases}. \quad (8)$$

$R \in \mathbb{R}^{\kappa \times \kappa}$ is an arbitrary rotation matrix. [Kunin et al., 2019] obtain similar optimal values for the regularized linear autoencoders. We can derive several interesting features of \widehat{W} :

1. It is possible to have $\text{rank}(\widehat{W}) < \kappa$. We use this observation in section 3.3 for the choice of the latent space size of the VAE.
2. The rotation matrix R is arbitrary. This implies that our optimal solution is invariant to rotations. [Dai et al., 2018] show this as well as invariance to permutations in their theorem 2.

It can be shown that other candidate points of $\widehat{\mathcal{L}}(W, b)$ for W represent saddle points (see appendix of [Tipping and Bishop, 1999]). So, if we think of training a VAE, the optimizer should be robust to saddle points.

It is important that we assume X_1, \dots, X_d given Z are mutually independent with (2) and not that the X_1, \dots, X_d are mutually independent with

$$X \sim \text{Bern}(p_\theta). \quad (9)$$

S from (5) with b as in (6) is the sample covariance matrix for the variable $4Y := 4(X - 1/2\mathbb{1})$. If we take the expectation under assumption (9), with X_1, \dots, X_d mutually independent, we get

$$\begin{aligned} \mathbb{E}(S) &= 16 \cdot \text{diag}(\text{Var}(X_1), \dots, \text{Var}(X_d)) \\ &= 16 \cdot \text{diag}(p_{\theta,1} \cdot (1 - p_{\theta,1}), \dots, p_{\theta,d} \cdot (1 - p_{\theta,d})). \end{aligned}$$

So, we have all the eigenvalues $\lambda_1, \dots, \lambda_d$ of $\mathbb{E}(S)$ readily at hand and λ_j only depends on $p_{\theta,j} \in [0, 1]$ for $j = 1, \dots, d$. The inequality in (8) is only fulfilled at $p_{\theta,j} = 0.5$, which results in $\widehat{W} = \mathbf{0}$. Thus assumption (9), with X_1, \dots, X_d mutually independent, does not lead to meaningful solutions for the weights of the decoder.

Under assumption (2), with X_1, \dots, X_d given Z mutually independent, we cannot calculate $\mathbb{E}(S)$ as above: X_1, \dots, X_d are not mutually independent without knowing Z . This fact stems from the common parent argument in Bayesian network theory.

We generate data in 4.1 according to assumption (2). For this data we observe eigenvalues that are bigger than the needed value of 4.[‡]

Apart from the optimal W and b we achieve representations for optimal $\mu_z^{(i)}$ and $\Sigma_z^{(i)}$:

[‡]E.g.: 8.44, 5.96, 5.42,

Corollary 1. For an observation $x^{(i)} \in \{0, 1\}^d$ the optimal closed form solutions for $\mu_z^{(i)}$ and $\Sigma_z^{(i)}$ of the lower bound of the ELBO are given by

$$\hat{\Sigma}_z := \hat{\Sigma}_z^{(i)} = (I_\kappa + \frac{1}{4}W^TW)^{-1}, \quad (10)$$

and

$$\begin{aligned} \hat{\mu}_z^{(i)} &= \hat{\Sigma}_z W^T \left(x^{(i)} - \frac{1}{2}\mathbf{1} - \frac{1}{4}b \right) \\ &= \hat{\Sigma}_z W^T \left(y^{(i)} - \frac{1}{4}b \right). \end{aligned} \quad (11)$$

These optimal solutions are a by-product of the proof of proposition 1. They give us insight into what to expect from a trained neural net. We use this to propose a new initialization and a change of the VAE structure.

3.2 Initialization and change of net architecture for Bernoulli VAE

Given the optimal values for the encoder outputs in corollary 1 as well as for the decoder parameters in (7) and (6), we initialize the corresponding weights and biases of a VAE. This affects only the last layers of the encoder and decoder. Then we introduce and discuss a slight change of the net architecture. At last we explain our approach for over-parametrized nets in the form that we have more ingoing dimensions into the last layers of encoder and decoder than needed. This issue arises when we consider hidden layers with higher dimension than the input.

Our simulation results in 4.3 show a faster convergence and comparable results as produced by a VAE without this change.

The weights and biases for the last decoder layer are straightforward set as the optimal \hat{W} from (7) and \hat{b} from (6). For the last encoder layers we first note that there are two layers: the “ μ_z ”- and the “ $\log \sigma_z^2$ ”-layer. We initialize the weights and biases of the “ μ_z ”-layer as follows:

- $\hat{W}_e := \hat{\Sigma}_z \hat{W}^T$.
- $\hat{b}_e := \hat{\Sigma}_z \hat{W}^T \left(-\frac{1}{2}\mathbf{1} - \frac{1}{4}\hat{b} \right)$.

The VAE-architecture is changed at the “ $\log \sigma_z^2$ ”-layer: We decouple it from the layers before. Consequently, the output of this layer never changes. We set it to produce the log of $\text{diag}(\hat{\Sigma}_z)$. This change is justified by the fact that $\hat{\Sigma}_z$ in (10) is the same for all inputs $x^{(i)}$. Apart from a better initialization than over random values, a benefit of this approach is that the Z distribution now is prohibited to become degenerated. E.g. is this the case when $\Sigma_z \rightarrow \mathbf{0}$.

All weights and biases produced here only depend on \hat{W} and \hat{b} , which are easily obtainable: We just need to calculate the sample mean and a Singular Value Decomposition of the sample covariance.

In case of over-parametrized nets, more edges lead into the affected layers than we need. This problem only concerns the weights and not the biases. We solve this by initializing not needed dimensions of the weights with zero. This still allows the net to change these weights during training, but they have a starting point which is optimal in the sense of our bound from proposition 1.

3.3 Optimal latent space size

Given the structure of \hat{W} in (7), we propose a decision support for the choice of the latent space dimension κ . The approach we propose here is based on PCA and is therefore not new. Usually we perform a Singular Value Decomposition of the estimated covariance matrix and consider the dimensions associated to the biggest eigenvalues. This way, we retain the variation present in the data up to a maximum amount. The parameter κ equals the number of eigenvalues we decide for.

The form of (7) shows which eigenvalues of the sample covariance matrix S are eligible for \hat{W} : Only those that are greater than 4. Hence, all dimensions with smaller associated eigenvalues can be discarded as this would only introduce a zero-row in \hat{W} .

Concluding, the value for κ can be chosen the following way:

1. Create S as in (5) with b as in (6).

2. Perform a Singular Value Decomposition of S .
3. Only consider eigenvalues as eligible that are greater than 4 when choosing κ

For the equivalent terms in [Tipping and Bishop, 1999], [Dai et al., 2018] and [Kunin et al., 2019], this approach is not directly possible. There, \hat{W} also depends on the parameter σ_x^2 , the variance of the observation distribution under isotropic Gaussian assumption. This parameter has to be estimated.

4 Simulation

Given our theoretical results, we provide simulations that back up these findings. Therefore, in this section, we compare performances of VAEs. The essential messages of our simulations are the following:

1. Given a VAE, our proposed initialization of the net results in a faster training convergence.
2. Even without our initialization as starting points, the VAE approaches the theoretical bound after a longer training period.
3. With our initialization and architecture, the VAE is less prone to over-fitting.

For the simulations, we generate data and show that our theory applies to the general case. Practitioners are welcome to apply our proposed setting to their data.

We first describe the data generation in detail. Then, we show the architecture and the initialization of the VAE and how we train the two resulting nets. Given these two parts, we present the simulation setup and interpret the results.

4.1 Data generation

For $k = 2$, $N \in \{100; 5000; 10000\}$ and $d \in \{200; 400; 1000\}$ we generate two matrices $A \in \mathbb{R}^{N \times k}$ and $B \in \mathbb{R}^{d \times k}$. A is identifiable with the principal components and B with the loading vectors of a PCA. B is assumed to be sparse (see below).

We construct the matrices in the fashion of [Lee et al., 2010]: The two-dimensional principal components $a^{(i)}$ ($i = 1, \dots, N$) of A are drawn from normal distributions, so that $a_1^{(i)} \sim \mathcal{N}(0, 0.09)$ and $a_2^{(i)} \sim \mathcal{N}(0, 0.25)$. The sparse loading vectors are constructed by setting B to zero except for $b_{j,1} = 1, j = 1, \dots, 20$ and $b_{j,2} = 1, j = 21, \dots, 40$.

Given A and B we calculate

$$\Xi := A \cdot B^T$$

and the probability matrix Π , with

$$\Pi = \sigma(\Xi),$$

where we apply the sigmoid function $\sigma(\cdot)$ element-wise. We then use the probabilities $\Pi_j^{(i)}$ to independently draw samples

$$x_j^{(i)} \sim \text{Bern}(\Pi_j^{(i)})$$

and with the data $X_{Data} := (x_j^{(i)})_{i=1, \dots, N; j=1, \dots, d}$, we conduct the simulation.

Given the combinations of N and d , we get nine different data sets for our simulation.

Though the case $N = 100$ seems to be rather odd for training of neural nets, [Lee et al., 2010] generate data explicitly with $N = 100$ and $d \in \{200; 400; 1000\}$ and denote it as challenging tasks for their logistic PCA. We therefore keep it in our simulation study to see how our bound from proposition 1 relates to the loss of the VAEs for the test data.

4.2 VAE architecture

The architecture of the VAE that we look at can be described as follows:

$$x(d) \rightarrow E_1(2000) \rightarrow E_2(1000) \rightarrow \mu_z(k) \rightarrow D_1(1000) \rightarrow D_2(2000) \rightarrow \hat{x}(d),$$

$$\searrow \log \sigma_z^2(k) \nearrow$$

where the dots just indicate the line break. Each aspect denotes a layer and the value in the parentheses gives the dimension of this layer. So, E_1, E_2 denote the hidden layers of the encoder and D_1, D_2 those of the decoder. This architecture, the notation and the training parameters (see next section) are as in [Dai et al., 2018].

The hidden layers of the encoder and the decoder are implemented with “ReLU”-activation (see [Nair and Hinton, 2010]), which is known to be highly expressive. The “ μ_z ”- and “ $\log \sigma_z^2$ ”- layer have linear activations. As we need an output between zero and one and in consistency with our theoretical derivation from before, the last layer “ \hat{x} ” has a sigmoid activation function.

The network weights and biases are initialized as proposed by [He et al., 2015]. This initialization particularly considers rectifier non-linearities.

Apart from the fact that we expect the net to provide a better loss than provided by our theoretical bound, the net should also be able to represent the optimal $\hat{\mu}_z^{(i)}$ and diagonal entries of the optimal $\hat{\Sigma}_z^{(i)}$ from corollary 1 if necessary.

We train a second version of VAE, called “VAE preinit”. This is equal to the one described above for all but the following two aspects:

1. We initialize the weights and biases of the “ μ_z ”- and “ \hat{x} ”-layer as proposed in 3.2. Dimensions that we do not need for this initialization are set to zero but can change during training.
2. We fix the “ $\log \sigma_z^2$ ”-layer to always produce the diagonal entries of $\hat{\Sigma}_z$ from corollary 1. The output of this layer is not affected by training. So the variance of “VAE preinit” does not depend on the input and behaves approximately as suggested from the theoretical results.

Obviously both autoencoders are over-parametrized for the simple simulation. Looking at the decoder part and comparing it with the data generation in 4.1, one layer suffices. Furthermore, our theoretical setting in section 3 manifests this view. We note that the simulation on such a “canonical” version of a VAE produced results that favoured our proposed initialization and architecture even more than those stated in 4.3. The results for this case can be found in the supplementary materials. The intention behind the over-parametrized structures is to show that even for deep learning architectures, our initialization performs well and that our theoretical bound serves its purpose.

4.3 Training setting and results

For training of the nets we used the Adam optimizer by [Kingma and Ba, 2015] with learning rate 0.0001 and a batch size of 100. Training was done for a total of 400 epochs each time. We split the data into 2/3 training data and 1/3 test data and calculate the optimal values \hat{W} , \hat{b} , $\hat{\mu}_z$ and $\hat{\Sigma}_z$ only on basis of the training data. Given these, we obtain a theoretical bound $\hat{\mathcal{L}}$ for training and test data. We also use these parameters for the initialization of “VAE preinit” described in 4.2.

We first present our simulation results given the values of the losses after the 400 epochs. Afterwards, we compare the development of the two autoencoders during one training.

4.3.1 Simulation results for deep architectures

Given the possible combinations of $d \in \{200; 400; 1000\}$ and $N \in \{100; 5.000; 10000\}$, we have nine different simulations. We generate data once and for each of the nine simulation settings we train the two VAEs with 100 different (randomly) initialized starting points. The “VAE preinit” layers affected by our initialization keep their values. For this net we get different (randomly) initialized starting points for the remaining layers.

Each simulation (200 net trainings) was executed on a Dual Intel Xeon Gold 6132 (“Skylake”) @ 2.6 GHz with 28 CPU cores. The longest setup ($N = 10000$ and $d = 4000$) took about two and a half days of computing time. We used and modified the implementation of a VAE provided by [Chollet and Others, 2015].[§]

Table 1 and table 2 display information on loss values at the end of 400 epochs of training. We calculate the deviation from the bound value displayed in the same row and provide the interval of minimal and maximal deviation, displayed as “[Min%,Max%]”.[¶] The “[Min%,Max%]” intervals let us highlight the main aspects later on better than a “mean \pm std”-format. The mean and standard deviation values for the deep leaning architectures can be found in the supplementary material. We also present the simulation results (“[Min%,Max%]” and “mean \pm std”) for the “canonical” architectures there.

[§]Our code together with a readme file for execution can be found in the provided file “vae_analysis_binary.zip” in the supplementary materials.

[¶]To recover the real minimal or maximal value calculate $-\hat{\mathcal{L}} \cdot (1 + \text{deviation in } \%)$: e.g. $134.52 \cdot (1 - 16.02\%) \approx 112.97$

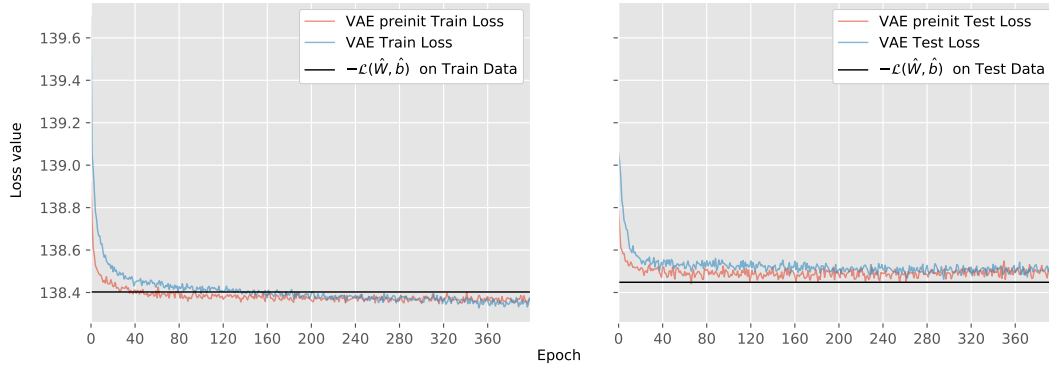


Figure 2: The figure displays the behaviour of the loss of VAEs as constructed in 4.2 over 400 epochs of training. The data was generated as in 4.1 with $N = 10000$ and $d = 200$. On the left we see the performance on the training set and on the right on the test set. The derived upper bound (for the negative of the average ELBO) is in both cases displayed as a black line.

In table 1 and table 2, the nets perform better with smaller values. A negative percentage means that the final loss is smaller than the bound. As stated earlier, the deep architecture we look at here is actually not comparable to the bound. Hence, the loss values can be greater than the bound.

Looking at the tables 1 and 2, we draw the following four conclusions:

1. Comparing the test cases, we favour “VAE preinit” in all but one setup $d = 1000$ and $N = 10000$.
2. For the simulation setups with $N = 100$ both nets are over-fitting. For all cases the “VAE preinit” is less prone to this behaviour, as can explicitly be seen from the performance on the test data in table 1.
3. For the training data, the bound is often reached by both nets. For the test data though, the resulting loss is likely to lie above the bound.
4. Overall, the intervals are getting tighter for increasing N : Not surprisingly more data results in better fits. The bound is more robust: The values for different N are comparable.

4.3.2 Loss development for deep architectures

Figure 2 displays loss values of the two different VAEs for test and training data. Furthermore, the bound $-\widehat{\mathcal{L}}(\widehat{W}, \widehat{b})$ was calculated for these two sets and added to the figure. As we are looking at the losses (the negative average ELBOs) of neural nets, smaller is better. We note that the “VAE preinit” has a faster convergence for both training and test set. After 400 epochs, the different net architectures produce comparable losses. We conclude that fixing the “ $\log \sigma_z^2$ ”-layer in “VAE preinit” produces a comparable final loss value. For the training set, both net architectures admit the bound $-\widehat{\mathcal{L}}(\widehat{W}, \widehat{b})$ after enough steps of training. Even though our theory from section 3 produces this bound for less parametrized net-structures than we look at here.

5 Conclusion and possible extensions

The derived theoretical bound for VAE is easy to calculate and we show that even the performance of deep VAE-architectures (six layers) can be assessed with it. Therefore, we propose to use our bound to monitor the training of Bernoulli VAE.

Using our proposed initialization and the modification of the Bernoulli VAE architecture, a faster convergence rate is visible. Furthermore, we get more favourable results for the final loss values in all but one of our simulations. As a result, we motivate practitioners with real world binary data to apply a Bernoulli VAE with this initialization and architecture to their data.

The decision support for the optimal latent dimension κ reduces the set of possible values when using a PCA.

Table 1: The table shows performances on the test data for deep learning architectures. For each net, we look at the information of 100 loss values after 400 epochs of training. The values displayed are the minimal and maximal relative deviations from the bound provided in the same row. They are displayed as “[Min%,Max%]”.

SIM.	$-\hat{\mathcal{L}}$	VAE PREINIT	VAE
D=200; N=100	139.34	[5.66%;12.66%]	[9.02%;22.08%]
D=200; N=5000	138.48	[0.01%;0.11%]	[0.10%;0.20%]
D=200; N=10000	138.45	[-0.01%;0.05%]	[0.02%;0.07%]
D=400; N=100	279.08	[5.69%;12.68%]	[7.97%;17.19%]
D=400; N=5000	277.22	[0.04%;0.09%]	[0.24%;0.31%]
D=400; N=10000	277.11	[0.02%;0.05%]	[0.02%;0.11%]
D=1000; N=100	694.80	[5.55%;11.81%]	[6.92%;15.33%]
D=1000; N=5000	693.25	[0.08%;0.13%]	[0.02%;0.35%]
D=1000; N=10000	693.12	[0.02%;0.04%]	[0.00%;0.02%]

Table 2: The table shows performances on the training data for deep learning architectures. For a description see the caption of table 1.

SIM.	$-\hat{\mathcal{L}}$	VAE PREINIT	VAE
D=200; N=100	134.52	[-16.02%;-11.58%]	[-25.76%;-21.81%]
D=200; N=5000	138.35	[-0.09%;-0.03%]	[-0.13%;-0.06%]
D=200; N=10000	138.39	[-0.04%;-0.01%]	[-0.06%;-0.02%]
D=400; N=100	269.59	[-22.43%;-17.28%]	[-29.72%;-24.42%]
D=400; N=5000	276.91	[-0.25%;-0.14%]	[-0.41%;-0.30%]
D=400; N=10000	276.99	[-0.06%;-0.03%]	[-0.10%;0.01%]
D=1000; N=100	674.44	[-27.56%;-22.05%]	[-32.76%;-27.03%]
D=1000; N=5000	692.54	[-0.59%;-0.44%]	[-0.55%;0.00%]
D=1000; N=10000	692.75	[-0.19%;-0.04%]	[0.02%;0.05%]

References

- [Baldi and Hornik, 1989] Baldi, P. and Hornik, K. (1989). Neural networks and principal component analysis: Learning from examples without local minima. *Neural Networks*, 2(1):53–58.
- [Blaschke et al., 2018] Blaschke, T., Olivecrona, M., Engkvist, O., Bajorath, J., and Chen, H. (2018). Application of Generative Autoencoder in De Novo Molecular Design. *Molecular Informatics*, 37(1-2).
- [Bourlard and Kamp, 1988] Bourlard, H. and Kamp, Y. (1988). Auto-Association by Multilayer Perceptrons and

- Singular Value Decomposition. *Biol. Cybern.*, 59:291–294.
- [Chollet and Others, 2015] Chollet, F. and Others (2015). Keras.
- [Collins et al., 2002] Collins, M., Dasgupta, S., and Schapire, R. E. (2002). A Generalization of Principal Component Analysis to the Exponential Family. In *Advances in neural information processing systems*, pages 617—624.
- [Dai et al., 2018] Dai, B., Wang, Y., Aston, J., and Wipf, D. (2018). Connections with Robust PCA and the Role of Emergent Sparsity in Variational Autoencoder Models. *Journal of Machine Learning Research*, 19:1–42.
- [de Leeuw, 2006] de Leeuw, J. (2006). Principal component analysis of binary data by iterated singular value decomposition. *Computational Statistics & Data Analysis*, 50(1):21–39.
- [Duan et al., 2019] Duan, X., Liu, J., and Zhang, E. (2019). Efficient image encryption and compression based on a VAE generative model. *Journal of Real-Time Image Processing*, 16(3):765–773.
- [Germain et al., 2015] Germain, M., Gregor, K., Murray, I., and Larochelle, H. (2015). Made: Masked autoencoder for distribution estimation. In *Proceedings of the 32nd International Conference on Machine Learning, Lille, France JMLR: W&CP volume 37*, volume 2, pages 881–889. International Machine Learning Society (IMLS).
- [Goodfellow et al., 2016] Goodfellow, I., Bengio, Y., and Courville, A. (2016). *Deep learning*.
- [He et al., 2015] He, K., Zhang, X., Ren, S., and Sun, J. (2015). Delving Deep into Rectifiers: Surpassing Human-Level Performance on ImageNet Classification. In *The IEEE International Conference on Computer Vision (ICCV)*.
- [Josse and Wager, 2016] Josse, J. and Wager, S. (2016). Bootstrap-Based Regularization for Low-Rank Matrix Estimation. *Journal of Machine Learning Research*, 17:1–29.
- [Kingma and Ba, 2015] Kingma, D. P. and Ba, J. L. (2015). Adam: A method for stochastic optimization. In *3rd International Conference on Learning Representations, ICLR 2015 - Conference Track Proceedings*. International Conference on Learning Representations, ICLR.
- [Kingma and Welling, 2014] Kingma, D. P. and Welling, M. (2014). Auto-Encoding Variational Bayes.
- [Kunin et al., 2019] Kunin, D., Bloom, J. M., Goeva, A., and Seed, C. (2019). Loss Landscapes of Regularized Linear Autoencoders. In *Proceedings of the 36th International Conference on Machine Learning*.
- [Landgraf and Lee, 2015] Landgraf, A. J. and Lee, Y. (2015). Dimensionality Reduction for Binary Data through the Projection of Natural Parameters. Technical report.
- [Lee et al., 2010] Lee, S., Huang, J. Z., and Hu, J. (2010). Sparse Logistic Principal Components Analysis For Binary Data. *The annals of applied statistics*, 4(3):1579–1601.
- [Makhzani et al., 2015] Makhzani, A., Shlens, J., Jaitly, N., Goodfellow, I., and Frey, B. (2015). Adversarial Autoencoders.
- [Nair and Hinton, 2010] Nair, V. and Hinton, G. E. (2010). Rectified linear units improve restricted boltzmann machines. In *Proceedings of the 27th international conference on machine learning (ICML-10)*, pages 807–814.
- [Pretorius et al., 2018] Pretorius, A., Kroon, S., and Kamper, H. (2018). Learning Dynamics of Linear Denoising Autoencoders. In *Proceedings of the 35th International Conference on Machine Learning*.
- [Saxe et al., 2014] Saxe, A. M., McClelland, J. L., and Ganguli, S. (2014). Exact solutions to the nonlinear dynamics of learning in deep linear neural networks. Technical report.
- [Tibshirani, 1996] Tibshirani, R. (1996). Regression Shrinkage and Selection Via the Lasso. *Journal of the Royal Statistical Society: Series B (Methodological)*, 58(1):267–288.
- [Tipping and Bishop, 1999] Tipping, M. E. and Bishop, C. M. (1999). Probabilistic Principal Component Analysis. *Journal of the Royal Statistical Society: Series B (Statistical Methodology)*, 61(3):611–622.
- [Zhao et al., 2019] Zhao, S., Song, J., and Ermon, S. (2019). InfoVAE: Balancing Learning and Inference in Variational Autoencoders. *Proceedings of the AAAI Conference on Artificial Intelligence*, 33(01):5885–5892.

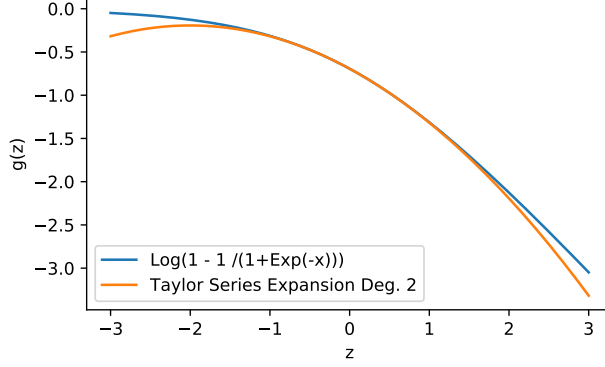


Figure 3: For the range -3 to 3 the Taylor series expansion of the function $\log(1 - \sigma(z))$, where $\sigma(\cdot)$ denotes the sigmoid function. The desired function is approximated from below by the degree 2 expansion.

A Supplementary Material

A.1 Proof of proposition 1

Proof. To proof proposition 1, we will change the perspective. Instead of maximizing the ELBO, we want to minimize the negative ELBO given by

$$\begin{aligned}
-\mathcal{L}(\phi, \theta) &:= \frac{1}{N} \sum_{i=1}^N D_{KL} \left(q_{\phi}(Z|x^{(i)}) || P(Z) \right) \\
&\quad - \mathbb{E}_{Z \sim q_{\phi}(\cdot|x^{(i)})} \left[\log P_{\theta}(x^{(i)}|Z) \right].
\end{aligned} \tag{12}$$

Looking at (12), we see two terms. For the KL-Divergence we have that

$$\begin{aligned}
2 \cdot D_{KL} \left(q_{\phi}(Z|x^{(i)}) || P(Z) \right) \\
= \text{tr}[\Sigma_z^{(i)}] - \log |\Sigma_z^{(i)}| + \|\mu_z^{(i)}\|_2^2 - \kappa
\end{aligned} \tag{13}$$

and for the second term (with q_{ϕ} as abbreviation for $q_{\phi}(\cdot|x^{(i)})$) we derive that

$$\begin{aligned}
& - \mathbb{E}_{q_{\phi}} \left[\log P_{\theta}(x^{(i)}|Z) \right] \\
&= - \mathbb{E}_{q_{\phi}} \left[\log \prod_{j=1}^d \left\{ p_{\theta,j}(z)^{x_j^{(i)}} (1 - p_{\theta,j}(z))^{(1-x_j^{(i)})} \right\} \right] \\
&= \mathbb{E}_{q_{\phi}} \left[-x^{(i)T} (WZ + b) \right] \\
&= \sum_{j=1}^d \mathbb{E}_{q_{\phi}} \left[\log \left(1 - \sigma \left([WZ + b]_j \right) \right) \right].
\end{aligned} \tag{14}$$

For the first term we have

$$\mathbb{E}_{q_{\phi}} [-x^{(i)T} (WZ + b)] = -x^{(i)T} (W\mu_z^{(i)} + b). \tag{15}$$

If we do a Taylor series expansion in the point $z_0 = 0$ for the function $g(z) := \log(1 - \sigma(z))$ we get

$$g(z) = -\log(2) - \frac{z}{2} - \frac{z^2}{8} + R_2(g, 0; z).$$

This approximation is shown in figure 3. A degree 2 expansion seems reasonable and we see that it is approaching the original function from below. In fact, we have that for the remainder $R_2(g, 0; z)$ it holds

$$R_2(g, 0; z) \geq 0 \quad \forall z \in \mathbb{R}.$$

An detailed argument is given section A.2.

Leaving the remainder aside, we get for the expectation in (14) that

$$\begin{aligned} \mathbb{E}_{q_\phi} \left(\log \left(1 - \sigma \left([WZ + b]_j \right) \right) \right) &\geq \\ -\log(2) - \frac{\mathbb{E}_{q_\phi}([WZ + b]_j)}{2} - \frac{\mathbb{E}_{q_\phi}([WZ + b]_j^2)}{8}. \end{aligned}$$

We can write $Z = \mathbf{S}_z^{(i)} Y + \boldsymbol{\mu}_z^{(i)}$, with $Y \sim \mathcal{N}(\vec{\mathbf{0}}, \mathbf{I})$. Therefore, if $W_{j\cdot}$ denotes the j -th row of W , for

$$[WZ + b]_j = W_{j\cdot} \mathbf{S}_z^{(i)} Y + W_{j\cdot} \boldsymbol{\mu}_z^{(i)} + b_j$$

it follows that

$$\mathbb{E}_{q_\phi}([WZ + b]_j) = W_{j\cdot} \boldsymbol{\mu}_z^{(i)} + b_j \tag{16}$$

and

$$\mathbb{E}_{q_\phi}([WZ + b]_j^2) = W_{j\cdot} \boldsymbol{\Sigma}_z^{(i)} W_{j\cdot}^T + (W_{j\cdot} \boldsymbol{\mu}_z^{(i)} + b_j)^2. \tag{17}$$

For the sum in (14), we get

$$\begin{aligned} &\sum_{j=1}^d \mathbb{E}_{q_\phi}[\log \sigma([WZ + b]_j)] \\ &\geq -d \log(2) - \frac{1}{2} \mathbf{1}^T W \boldsymbol{\mu}_z^{(i)} - \frac{1}{2} \mathbf{1}^T b \\ &\quad - \frac{1}{8} \text{tr}(W \boldsymbol{\Sigma}_z^{(i)} W^T) - \frac{1}{8} \|W \boldsymbol{\mu}_z^{(i)}\|_2^2 \\ &\quad - \frac{1}{4} b^T W \boldsymbol{\mu}_z^{(i)} - \frac{1}{8} \|b\|_2^2, \end{aligned}$$

with $\mathbf{1} = (1, \dots, 1)^T \in \mathbb{R}^d$. We always approximate the sum from below and hence the negative ELBO from above. Putting these results together with (13) and (15) for our target function in (12), it follows that it is smaller than

$$\begin{aligned} -\widehat{\mathcal{L}}(\phi, W, b) &:= \frac{1}{N} \sum_{i=1}^N \left[\frac{\text{tr}[\boldsymbol{\Sigma}_z^{(i)}]}{2} - \frac{\log |\boldsymbol{\Sigma}_z^{(i)}|}{2} + \frac{\|\boldsymbol{\mu}_z^{(i)}\|_2^2}{2} \right. \\ &\quad - \frac{\kappa}{2} - x^{(i)T} (W \boldsymbol{\mu}_z^{(i)} + b) \\ &\quad + d \log(2) + \frac{1}{2} \mathbf{1}^T W \boldsymbol{\mu}_z^{(i)} + \frac{1}{2} \mathbf{1}^T b \\ &\quad + \frac{1}{8} \text{tr}(W \boldsymbol{\Sigma}_z^{(i)} W^T) + \frac{1}{8} \|W \boldsymbol{\mu}_z^{(i)}\|_2^2 \\ &\quad \left. + \frac{1}{4} b^T W \boldsymbol{\mu}_z^{(i)} + \frac{1}{8} \|b\|_2^2 \right]. \end{aligned}$$

All potential minima w.r.t. $\boldsymbol{\Sigma}_z^{(i)}$ have to conform to

$$\widehat{\boldsymbol{\Sigma}}_z := \widehat{\boldsymbol{\Sigma}}_z^{(i)} = (I_\kappa + \frac{1}{4} W^T W)^{-1}, \tag{18}$$

independent of $x^{(i)}$. To see that these are also minima and not maxima, consider that it holds (see A.3) that

$$\kappa + \log |AA^T| = \min_{\Gamma > 0} \text{tr}(AA^T \Gamma^{-1}) + \log |\Gamma|,$$

where we set $\Gamma^{-1} = \boldsymbol{\Sigma}_z$ and $AA^T = I_\kappa + \frac{1}{4} W^T W$.

Given $\hat{\Sigma}_z$ the candidates for the minimal target function are writeable as

$$\begin{aligned} -\widehat{\mathcal{L}}(\phi \setminus \{\Sigma_z\}, W, b) &= \frac{1}{N} \sum_{i=1}^N \left[\left(-x^{(i)} + \frac{1}{2}\mathbb{1} + \frac{1}{4}b \right)^T W \boldsymbol{\mu}_z^{(i)} + \frac{\|\boldsymbol{\mu}_z^{(i)}\|_2^2}{2} \right. \\ &\quad \left. + \frac{1}{8} \|W \boldsymbol{\mu}_z^{(i)}\|_2^2 + (-x^{(i)} + \frac{1}{2}\mathbb{1})^T b + \frac{1}{8} \|b\|_2^2 \right. \\ &\quad \left. + \frac{1}{2} \log |I_\kappa + \frac{1}{4} W^T W| + d \log(2) \right]. \end{aligned}$$

For $\boldsymbol{\mu}_z^{(i)}$, we achieve as minimal points

$$\begin{aligned} \hat{\boldsymbol{\mu}}_z^{(i)} &= \hat{\Sigma}_z W^T \left(x^{(i)} - \frac{1}{2}\mathbb{1} - \frac{1}{4}b \right) \\ &= \hat{\Sigma}_z W^T \left(y^{(i)} - \frac{1}{4}b \right) \end{aligned} \tag{19}$$

with $y^{(i)} := \left(x^{(i)} - \frac{1}{2}\mathbb{1} \right) \in \left\{ -\frac{1}{2}, \frac{1}{2} \right\}^d$. These are minima since the second derivative is $\hat{\Sigma}^{-1}$, which is positive definite. Given the optimal $\boldsymbol{\mu}_z^{(i)}$ and $\Sigma_z^{(i)}$ our target function is only dependent on the parameters W and b . Hence

$$\begin{aligned} -\widehat{\mathcal{L}}(W, b) &= \frac{1}{N} \sum_{i=1}^N \left[\left(y^{(i)} - \frac{1}{4}b \right)^T E \left(y^{(i)} - \frac{1}{4}b \right) - y^{(i)T} b \right] \\ &\quad + \frac{1}{8} \|b\|_2^2 + \frac{1}{2} \log |I_\kappa + \frac{1}{4} W^T W| + d \log(2), \end{aligned} \tag{20}$$

where $E := W \left(\frac{1}{2} \hat{\Sigma}_z^2 - \hat{\Sigma}_z + \frac{1}{8} \hat{\Sigma}_z W^T W \hat{\Sigma}_z \right) W^T$ and $\hat{\Sigma}_z$ is fixed. Consider the Singular Value Decomposition of $W = U \tilde{D} V^T$ with $U \in \mathbb{R}^{d \times d}$ and $V \in \mathbb{R}^{\kappa \times \kappa}$ are unitary matrices and

$$\tilde{D} = \begin{bmatrix} d_1 & \dots & 0 \\ \vdots & \ddots & \vdots \\ 0 & \dots & d_\kappa \\ \vdots & \ddots & \vdots \\ 0 & \dots & 0 \end{bmatrix} \in \mathbb{R}^{d \times \kappa}.$$

We have

$$\tilde{D}^T \tilde{D} = \begin{bmatrix} d_1^2 & \dots & 0 \\ \vdots & \ddots & \vdots \\ 0 & \dots & d_\kappa^2 \end{bmatrix}$$

and can therefore write

$$\begin{aligned} \hat{\Sigma}_z &= \left(V \left(I_\kappa + \frac{1}{4} \tilde{D}^T \tilde{D} \right) V^T \right)^{-1} \\ &= V \hat{D} V^T, \end{aligned}$$

with $\hat{D} := \text{diag} \left(\frac{4}{4 + d_1^2}, \dots, \frac{4}{4 + d_\kappa^2} \right)$. For the matrix expression in the middle of the term in (20) it follows that

$$\begin{aligned} &W \left(\frac{1}{2} \hat{\Sigma}_z^2 - \hat{\Sigma}_z + \frac{1}{8} \hat{\Sigma}_z W^T W \hat{\Sigma}_z \right) W^T \\ &= W \left(V \left(\frac{1}{2} \hat{D}^2 - \hat{D} + \frac{1}{8} \hat{D} \tilde{D}^T \tilde{D} \hat{D} \right) V^T \right) W^T \\ &= W \left(V \check{D} V^T \right) W^T, \end{aligned} \tag{21}$$

where we denote $\check{D} = \text{diag}\left(\frac{-2}{4+d_1^2}, \dots, \frac{-2}{4+d_\kappa^2}\right)$. The justification of the last equation becomes apparent, when we consider one respective diagonal element d . of the diagonal matrices in the equation. We have

$$\begin{aligned} & \frac{1}{2} \frac{16}{(4+d^2)^2} - \frac{4}{4+d^2} + \frac{1}{8} \frac{16d^2}{(4+d^2)^2} \\ &= \frac{8}{(4+d^2)^2} - \frac{16+4d^2}{(4+d^2)^2} + \frac{2d^2}{(4+d^2)^2} \\ &= \frac{-8-2d^2}{(4+d^2)^2} \\ &= \frac{-2}{(4+d^2)}. \end{aligned}$$

We can further rewrite (21) as

$$\begin{aligned} W(V\check{D}V^T)W^T &= U\check{D}\check{D}\check{D}^T U^T \\ &=: -UDU^T, \end{aligned}$$

where we have introduced

$$D := \begin{bmatrix} \text{diag}\left(\frac{2d_1^2}{4+d_1^2}, \dots, \frac{2d_\kappa^2}{4+d_\kappa^2}\right) & \mathbf{0} \\ \mathbf{0} & \mathbf{0} \end{bmatrix} \in \mathbb{R}^{d \times d}.$$

So for our target function in (20), we get

$$\begin{aligned} -\widehat{\mathcal{L}}(W, b) &= \frac{1}{N} \sum_{i=1}^N \left[-\left(y^{(i)} - \frac{1}{4}b\right)^T UDU^T \left(y^{(i)} - \frac{1}{4}b\right) - y^{(i)T} b \right] \\ &\quad + \frac{1}{8} \|b\|_2^2 + \frac{1}{2} \log |I_\kappa + \frac{1}{4}W^T W| + d \log(2). \end{aligned}$$

By adding and subtracting the constant term $\frac{1}{N} \sum_{i=1}^N 2\|y^{(i)}\|_2^2 = \frac{d}{2}$, concluding

$$2\|y^{(i)}\|_2^2 - \frac{4}{4} y^{(i)T} b + \frac{2}{8 \cdot 2} \|b\|_2^2 = 2 \cdot \left(y^{(i)} - \frac{1}{4}b\right)^T \left(y^{(i)} - \frac{1}{4}b\right)$$

and together with

$$\frac{1}{2} \log |I_\kappa + \frac{1}{4}W^T W| + d \log(2) = \frac{1}{2} \log |4I_d + WW^T|,$$

we get

$$\begin{aligned} -\widehat{\mathcal{L}}(W, b) &= \frac{1}{N} \sum_{i=1}^N \left[\left(y^{(i)} - \frac{1}{4}b\right)^T U(2I_d - D)U^T \left(y^{(i)} - \frac{1}{4}b\right) \right] \\ &\quad + \frac{1}{2} \log |4I_d + WW^T| - \frac{d}{2}. \end{aligned}$$

We can further rewrite

$$U(2I_d - D)U^T = \frac{16}{2} (4I_d + WW^T)^{-1}$$

and get

$$\begin{aligned} -\widehat{\mathcal{L}}(W, b) &= \frac{1}{N} \sum_{i=1}^N \left[\frac{1}{2} \left(4y^{(i)} - b\right)^T (4I_d + WW^T)^{-1} \left(4y^{(i)} - b\right) \right] \\ &\quad + \frac{1}{2} \log |4I_d + WW^T| - \frac{d}{2}. \end{aligned}$$

□

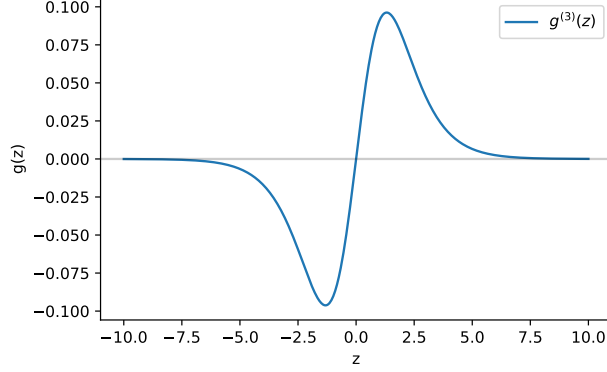


Figure 4: The third derivative of the function $g(z) := \log \sigma(z)$. It is point symmetric: For negative values it is negative and for positive values it is positive. The maximum/minimum is achieved at $\log(2 \pm \sqrt{3})$ and given by $z = \pm \frac{1}{6\sqrt{3}}$.

A.2 Analysing the Taylor Remainder

Let's have a look at the target term that we introduced when using a Taylor series expansion. The term we were considering is given by

$$\sum_{j=1}^d \mathbb{E}_{q_\phi} \left[\log \left(1 - \sigma \left([WZ + b]_j \right) \right) \right].$$

The Taylor series expansion in the point $z_0 = 0$ for the function $g(z) := \log(1 - \sigma(z))$ is

$$\log \sigma(z) = -\log(2) - \frac{z}{2} - \frac{z^2}{8} + R_2(g, 0; z),$$

where $R_2(g, 0; z)$ is the remainder of the expansion. It can be explicitly calculated as Lagrange Remainder

$$R_2(g, 0; z) = \frac{g^{(3)}(\xi)}{6} z^3 \tag{22}$$

with $g^{(3)}(\xi) = \frac{e^z(e^z - 1)}{(1 + e^z)^3}$ denoting the third derivative. ξ is a value between the expansion point 0 and z . This derivative is plotted in figure 4. It is point symmetric: For negative values it is negative and for positive values it is positive. Hence, the error that we make is always positive!

A.3 The maximum Entropy completion problem

Let $B, \Gamma \in \mathbb{R}^{\kappa \times \kappa}$ be symmetric positive definite matrices. Then it holds

$$B = \arg \min_{\Gamma > 0} \text{tr}(B\Gamma^{-1}) + \log |\Gamma|.$$

and hence

$$\kappa + \log |B| = \min_{\Gamma > 0} \text{tr}(B\Gamma^{-1}) + \log |\Gamma|.$$

Proof. Define the two distributions $\mathcal{N}_0(\boldsymbol{\mu}, B)$ and $\mathcal{N}_1(\boldsymbol{\mu}, \Gamma)$. We have

$$2 \cdot D_{KL}(\mathcal{N}_0(\boldsymbol{\mu}, B) || \mathcal{N}_1(\boldsymbol{\mu}, \Gamma)) = \text{tr}(B\Gamma^{-1}) + \log |\Gamma| - \kappa - \log |B| \tag{23}$$

Now, consider that for the Kullback-Leibler-Divergence with probability distributions P and Q it holds:

- $D_{KL}(P||Q) \geq 0$ for all inputs.
- $D_{KL}(P||Q) = 0$ if and only if $P = Q$ almost everywhere.

Hence, we conclude $B = \Gamma$ in the minimum. □

Table 3: The table shows performances on the test data for “canonical” architectures in the “[Min%,Max%]”-format. For a description, see table 1 and section 4.3.1.

SIM.	$-\widehat{\mathcal{L}}$	VAE PREINIT	VAE
D=200; N=100	138.94	[1.71%;2.47%]	[-0.20%;-0.05%]
D=200; N=5000	138.49	[-0.03%;0.05%]	[-0.01%;0.07%]
D=200; N=10000	138.46	[-0.02%;0.04%]	[-0.01%;0.06%]
D=400; N=100	278.53	[1.22%;1.61%]	[-0.49%;-0.38%]
D=400; N=5000	277.21	[0.00%;0.04%]	[0.00%;0.09%]
D=400; N=10000	277.13	[0.00%;0.02%]	[0.01%;0.03%]
D=1000; N=100	695.35	[1.11%;1.29%]	[-0.31%;-0.24%]
D=1000; N=5000	693.29	[0.02%;0.03%]	[0.01%;0.04%]
D=1000; N=10000	693.13	[0.00%;0.02%]	[0.00%;0.03%]

A.4 Simulation results for “canonical” architectures

Here, the test and training data results are provided for following cases:

- The “canonical” architecture with “[Min%,Max%]” format in table 3 and 4.
- The “canonical” architecture with “mean \pm std” format in table 5 and 6.
- The deep architecture with “mean \pm std” format in table 7 and 8.

For a description of the “[Min%,Max%]”-format see section 4.3.1. The “mean \pm std”-format presents the mean relative deviation (in %) and the std of this value.

The value of $-\widehat{\mathcal{L}}$ in the tables of “canonical”- architecture is different to the deep architecture due to a different seed during simulation.

A.5 Loss development for “canonical” net architectures

For both nets, we set the “canonical” VAE architecture as follows:

$$\begin{array}{c}
 x(d) \rightarrow E_1(2000) \rightarrow E_2(d) \rightarrow \mu_z(k) \rightarrow \hat{x}(d) \\
 \searrow \log \sigma_z^2(k) \nearrow
 \end{array}$$

This structure admits to the data generation in 4.1 and to our theoretical setting in 3.1.

The decoder resembles exactly the assumed structure in proposition 1. We still have several layers for the encoder in order to give the VAE the possibility to account for the assumptions in proposition 1.

With this architecture, for the “VAE preinit” we do not have to consider not needed dimensions as zero (as mentioned in 3.2) as there are none.

Figure 5 shows the results for training “canonical” versions of VAEs. We see how the “VAE preinit” directly adapts the assumed bound for the training case, where the high values at the beginning originate from the not readily initialized layers E_1 and E_2 of the encoder. The same holds for the test case.

For the training case, the normal VAE (initialized as in 4.2) takes a substantially longer time to adapt to the bound but eventually reaches it. For the test data case, we see that the normal VAE never performs at least as good as our lower bound indicates.

The “VAE preinit” is more favourable in both cases.

Table 4: The table shows performances on the training data for “canonical” architectures in the “[Min%,Max%]”-format. For a description, see table 1 and section 4.3.1.

SIM.	$-\hat{\mathcal{L}}$	VAE PREINIT	VAE
D=200; N=100	134.83	[-1.52%;-0.95%]	[2.47%;2.67%]
D=200; N=5000	138.35	[-0.06%;0.00%]	[-0.03%;0.05%]
D=200; N=10000	138.40	[-0.04%;0.00%]	[-0.03%;0.03%]
D=400; N=100	268.46	[-1.39%;-1.16%]	[2.80%;2.98%]
D=400; N=5000	276.90	[-0.04%;-0.01%]	[-0.02%;0.05%]
D=400; N=10000	276.99	[-0.02%;0.00%]	[-0.02%;0.01%]
D=1000; N=100	674.50	[-1.27%;-1.17%]	[2.10%;2.25%]
D=1000; N=5000	692.55	[-0.03%;-0.01%]	[-0.01%;0.01%]
D=1000; N=10000	692.76	[-0.02%;-0.01%]	[-0.01%;0.01%]

Table 5: The table shows performances on the test data for “canonical” architectures in the “mean \pm std”-format. For a description, see table 1 and section 4.3.1.

SIM.	$-\hat{\mathcal{L}}$	VAE PREINIT	VAE
D=200; N=100	138.94	2.02% \pm 0.15%	-0.12% \pm 0.03%
D=200; N=5000	138.49	0.01% \pm 0.02%	0.03% \pm 0.02%
D=200; N=10000	138.46	0.01% \pm 0.01%	0.02% \pm 0.01%
D=400; N=100	278.53	1.40% \pm 0.08%	-0.43% \pm 0.02%
D=400; N=5000	277.21	0.03% \pm 0.01%	0.02% \pm 0.01%
D=400; N=10000	277.13	0.01% \pm 0.01%	0.02% \pm 0.01%
D=1000; N=100	695.35	1.19% \pm 0.03%	-0.28% \pm 0.02%
D=1000; N=5000	693.29	0.02% \pm 0.00%	0.02% \pm 0.00%
D=1000; N=10000	693.13	0.01% \pm 0.00%	0.01% \pm 0.00%

Table 6: The table shows performances on the training data for “canonical” architectures in the “mean \pm std”-format. For a description, see table 1 and section 4.3.1.

SIM.	$-\widehat{\mathcal{L}}$	VAE PREINIT	VAE
D=200; N=100	134.83	-1.24% \pm 0.10%	2.55% \pm 0.04%
D=200; N=5000	138.35	-0.03% \pm 0.01%	0.02% \pm 0.01%
D=200; N=10000	138.40	-0.02% \pm 0.01%	0.00% \pm 0.01%
D=400; N=100	268.46	-1.26% \pm 0.04%	2.92% \pm 0.04%
D=400; N=5000	276.90	-0.02% \pm 0.01%	0.00% \pm 0.01%
D=400; N=10000	276.99	-0.01% \pm 0.00%	-0.01% \pm 0.00%
D=1000; N=100	674.50	-1.23% \pm 0.02%	2.17% \pm 0.03%
D=1000; N=5000	692.55	-0.02% \pm 0.00%	0.00% \pm 0.01%
D=1000; N=10000	692.76	-0.01% \pm 0.00%	-0.01% \pm 0.00%

Table 7: The table shows performances on the test data for deep architectures in the “mean \pm std”-format. For a description, see table 1 and section 4.3.1.

SIM.	$-\widehat{\mathcal{L}}$	VAE PREINIT	VAE
D=200; N=100	139.34	8.60% \pm 1.37%	14.70% \pm 2.34%
D=200; N=5000	138.48	0.06% \pm 0.02%	0.14% \pm 0.02%
D=200; N=10000	138.45	0.02% \pm 0.01%	0.05% \pm 0.01%
D=400; N=100	279.08	8.64% \pm 1.46%	12.04% \pm 1.76%
D=400; N=5000	277.22	0.07% \pm 0.01%	0.26% \pm 0.01%
D=400; N=10000	277.11	0.04% \pm 0.01%	0.09% \pm 0.02%
D=1000; N=100	694.80	8.73% \pm 1.40%	10.58% \pm 1.82%
D=1000; N=5000	693.25	0.09% \pm 0.01%	0.18% \pm 0.08%
D=1000; N=10000	693.12	0.03% \pm 0.00%	0.01% \pm 0.00%

Table 8: The table shows performances on the training data for deep architectures in the “mean ± std”-format. For a description, see table 1 and section 4.3.1.

SIM.	$-\hat{\mathcal{L}}$	VAE PREINIT	VAE
D=200; N=100	134.52	-14.36% ±0.88%	-23.45% ±0.77%
D=200; N=5000	138.35	-0.06% ±0.01%	-0.10% ±0.01%
D=200; N=10000	138.39	-0.03% ±0.01%	-0.04% ±0.01%
D=400; N=100	269.59	-19.89% ±1.08%	-27.44% ±0.96%
D=400; N=5000	276.91	-0.19% ±0.02%	-0.36% ±0.02%
D=400; N=10000	276.99	-0.05% ±0.01%	-0.07% ±0.02%
D=1000; N=100	674.44	-24.71% ±1.08%	-30.23% ±1.19%
D=1000; N=5000	692.54	-0.51% ±0.03%	-0.24% ±0.14%
D=1000; N=10000	692.75	-0.14% ±0.02%	0.04% ±0.01%

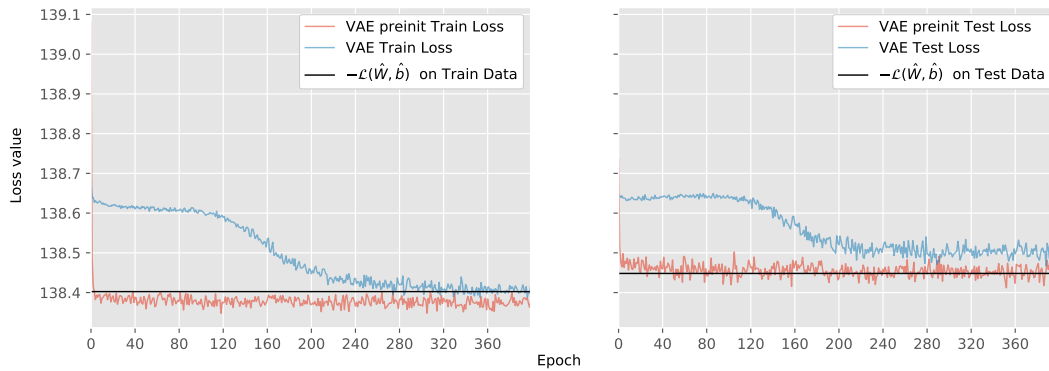


Figure 5: The figure displays the behaviour of the loss of the simple VAEs as constructed in A.5 over 400 epochs of training. The data is exactly as for figure 2. Further description can also be found there.